

Experimental study of quasi-elastic neutrino interactions on Ar with a liquid Ar TPC exposed to the WANF neutrino beam

A. Curioni^a *

^aPhysics Department, PO BOX 208120, Yale University, New Haven, CT, 06520-8120, USA

We present results from the first exposure of a liquid Ar time projection chamber to a neutrino beam. The data have been collected in 1997 with a 50 liter ICARUS-like chamber located between the CHORUS and NOMAD experiment at the CERN West Area Neutrino Facility. We focus on the analysis of quasi-elastic interactions; despite the limited size of the detector, nuclear effects beyond Fermi motion and Pauli blocking have been observed as perturbations to the pure quasi-elastic kinematics.

1. Introduction

In 1997 a liquid argon time projection chamber (LArTPC) with a fiducial volume of about 50 l was exposed to the multi-GeV wide-band neutrino beam of the CERN West Area Neutrino Facility (WANF) [1,2], during the NOMAD [3] and CHORUS [4] data taking. The LArTPC was placed on a platform 4.5 m high, between the CHORUS and NOMAD detectors. The modest size of the LArTPC fiducial volume (~ 50 liters) made necessary a muon spectrometer downstream the TPC. A coincidence with the NOMAD DAQ was set up to use the detectors located into the NOMAD magnetic dipole as a spectrometer. During the test 1.2×10^{19} p.o.t. were integrated, and about 10^5 triggers recorded. The test was run jointly by a group from Milano University and the ICARUS collaboration [6]. The data accumulated in 1997 still offer the unique opportunity of an experimental study on neutrino interactions on Ar nuclei. At this time of writing, final results from the experiment have not yet been reported in any systematic fashion (but see [7,8] for preliminary results and a more detailed description of the experimental apparatus); a comprehensive set of results from the 1997 test is presented here for the first time, while a more thorough and final paper is in preparation.

2. The experimental setup

The LArTPC had an active volume of $32 \times 32 \times 46.8 \text{ cm}^3$, enclosed in a stainless steel vessel in the shape of a bowed-bottom cylinder 90 cm high with a radius of 35 cm. The active volume contained 67 kg of liquid Ar. Ionization electrons produced by the passage of charged particles in liquid Ar drift toward the anode under the action of 214 V/cm uniform electric field. The readout electrodes are two parallel planes of wires running orthogonally; the planes are at a distance of 4 mm and each plane has 128 wires. Each stainless steel wire has a diameter of $100 \mu\text{m}$; the distance between the wires is 2.54 mm. The ionization electrons drift through the first (*induction*) wire plane so that the integrated induction signal is zero. The *collection* plane then collects the drifting electrons. The mean charge per unit pitch (2.54 mm) for a m.i.p. crossing the chamber parallel to the readout planes, corresponds to about 2.3×10^4 electrons ($\sim 4 \text{ fC}$).

The chamber has been exposed to the ν beam produced at the CERN WANF. The primary 450 GeV protons from the CERN SPS were extracted every 14.4 s in two spills (1.8×10^{13} protons per spill, on average) of 6 ms duration each and separated by 2.5 s, and hit a segmented Be target. Secondaries were selected in momentum and focused by a system of collimators and magnetic lenses. The experimental area was located 940 m downstream the target. The mean energy

*On behalf of the ICARUS-Milano collaboration

of the ν_μ reaching the detectors is 24.3 GeV, while contaminations from other flavors are below 7% for $\bar{\nu}_\mu$ and $\sim 1\%$ for ν_e [2].

The trigger was provided by a set of plastic scintillators, located downstream the chamber before the NOMAD apparatus. Incoming charged particles were vetoed by 5 large plastic scintillators mounted in front of the chamber and by the last scintillator plane of CHORUS, which vetoed particles deflected by the CHORUS magnetic field entering the chamber at large angles with respect to the nominal beam direction.

The local trigger required the coincidence of the SPS beam spill, at least one of the trigger scintillators, and the two trigger scintillator planes of NOMAD (T1 and T2 in [9]). Moreover, a trigger was rejected if the NOMAD acquisition system was in BUSY mode or if it came less than 500 μs after the previous trigger, inhibiting the occurrence of overlapping. In this configuration $\sim 11\%$ of the recorded events had a vertex in the fiducial volume of the TPC. The request of a charged particle triggering the chamber locally and reaching NOMAD up to T1 and T2 limited the useful data to ν_μ charged-current interactions.

3. Event reconstruction and particle identification

Interactions in the TPC fiducial volume were fully imaged in two 2D images with a common coordinate (time), with full calorimetric information associated with each point. The common coordinate allows an unambiguous 3D reconstruction of the event, at least for simple topologies. Each 2D-image represents the signal amplitude digitized by the ADC (in a linear gray scale) versus the time sample (drift coordinate) and the wire number. Fig. 1 shows the image of a quasi-elastic (QE) event in the induction and collection planes. Units are wire number versus drift time in μs . Appropriate filtering techniques have been applied to deconvolve the instrumental response and precisely associate the charge deposition to each pixel in the image. For the collection wires a universal response function has been determined empirically from events in the m.i.p. sample (elementary charge deposition). The response was

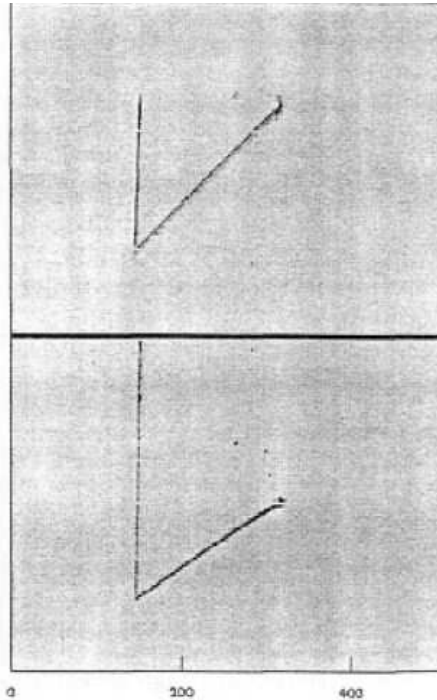


Figure 1. The filtered image of an event reconstructed as $\nu_\mu n \rightarrow \mu^- p$, with a m.i.p. leaving the TPC fiducial volume and an identified stopping proton. *Top* induction view; *bottom* collection view.

then deconvolved by means of a Discrete Fourier Analysis to reconstruct the topology of the actual charge deposition in the event. A different approach was adopted for the induction view, where the charge measurement in that view was not accomplished and only the event position, measured by the zero-crossing of the induced signal, was reconstructed.

3.1. Proton reconstruction and p/ π separation

For a proton, the identification and momentum measurement were performed using only information from the TPC. The discrimination between protons and charged pions is performed exploiting the different behavior of energy loss as a function

of the range. For the case of candidates stopping in the fiducial volume of the chamber, as the ones of the “golden sub-sample” considered in Sec.4, the discrimination is highly simplified: it is based on the consistency between the reconstructed kinetic energy from the range and the integrated charge deposited by the candidate along its path-length. For partially contained candidates, a much better assessment of the charge response of the TPC and of quenching effects[10] is required, since proton identification is based only on the visible pattern of the energy loss. Such events are not considered here. For fully contained protons, the momentum uncertainty is dominated by the finite pitch of the wires. The equivalent pitch in the vertical direction (drift direction) is much smaller due to the high sampling rate of the fast ADC (360 μm). For horizontal protons of $p = 400 \text{ MeV}/c$ the uncertainty is of the order of 7 MeV/c. The angular resolution in the collection or induction view depends on the number of wires N hit by the particle along its path; it is $\sigma \simeq 0.36\sqrt{12}/(2.54 N^{3/2})$, corresponding e.g. to 15 mrad for $N=10$.

3.2. Muon reconstruction

The kinematic reconstruction of the outgoing muons exploits the tracking capability of NOMAD. An event triggering the chamber will have at least one penetrating track reaching the T1 and T2 trigger scintillators bracketing the TRD of NOMAD [9]. The corresponding track, nearly horizontal at the entrance of the NOMAD drift chamber volume, is reconstructed with an average momentum precision of $\sigma_p/p \sim 0.05/\sqrt{L} \oplus 0.008p/L^{5/2}$, L being the visible range in the volume itself expressed in meters and p the particle momentum in GeV. A 10 GeV horizontal muon crossing all the chambers ($L \sim 5m$) is reconstructed with a precision of 2.2%. The reconstructed particle is traced back to the TPC accounting for the magnetic field and the presence of the forward NOMAD calorimeter. The latter introduces the dominant uncertainty on the muon transverse momentum, due to multiple scattering (MS) in iron (190 cm for a horizontal muon). For small scattering angles ($\theta \ll 1 \text{ rad}$) the MS uncertainty on the transverse momentum is inde-

pendent of p and it turns out to be $\sim 140 \text{ MeV}$. The correctness of the back-tracing procedure has been cross-checked comparing the direction angles of the particles belonging to the m.i.p. calibration sample as measured by the TPC with the corresponding quantity from NOMAD.

4. Analysis of quasi elastic ν_μ interaction

4.1. Event selection and rates

The commissioning of the detector ended in August 1997. After that, 1.21×10^{19} protons on target have been integrated. The trigger efficiency was monitored during data taking and its integrated value is 97%. Additional losses are due to the TPC (3%) and NOMAD (15%) dead time and to detector faults. The effective live-time was 75%. 81,000 events had been recorded and analyzed by visual scanning. A minimum-bias sample has been obtained requiring no more than two tracks exiting the chamber and an arbitrary number of contained tracks. This sample contains the *golden sample* of QE interactions and other samples used to validate the simulation for background estimation. The golden sample consists of events with an identified proton of kinetic energy (T_p) larger than 50 MeV fully contained in the TPC and one muon whose direction extrapolated from NOMAD matches the outgoing track in the TPC. The distance of the interaction vertex from any of the TPC walls has to be greater than 1 cm. The muon candidate track projected onto the wire plane must be longer than 12 wire pitches. The event is accepted even in the presence of other stopping particles, as far as their kinetic energy (in the proton hypothesis) does not exceed the T_p of the leading proton. If tracks other than the identified muon leave the TPC or at least one converted photon with energy greater than 10 MeV is present in the fiducial volume, the event is rejected. The tightness of these selections defines a very clear topology for visual scanning (Fig. 1).

The lower T_p cut combined with the request of containment is very severe since the chamber volume is small. On the other hand, at lower T_p the proton range is comparable with the wire pitch and neither the proton momentum nor the

interaction vertex can be reconstructed with due precision. Moreover, for $T_p > 50$ MeV the π^\pm/p misidentification probability is negligible. The golden sub-sample contains pure QE interactions ($\nu_\mu n \rightarrow \mu^- p$), an intrinsic background dominated by resonant productions followed by pion absorption in the nucleus ($\nu_\mu p \rightarrow \Delta^{++}\mu^- \rightarrow \mu^- p \pi^+$, $\nu_\mu n \rightarrow \Delta^+\mu^- \rightarrow \mu^- p \pi^0$) and an instrumental background due to unidentified π^0 's ($\nu_\mu n \rightarrow \Delta^+\mu^- \rightarrow \mu^- p \pi^0$). On the other hand, the $\nu_\mu n \rightarrow \Delta^+\mu^- \rightarrow \mu^- n \pi^+$ contamination is negligible in this tightly selected sample.

The efficiency of the selections for QE interactions and their intrinsic background has been evaluated by Monte Carlo experimentation based on the FLUKA code [11] and it turned out to be 17%. Similarly, MC provided the inefficiency of the vetoing selections for $\nu_\mu n \rightarrow \Delta^+\mu^- \rightarrow \mu^- p \pi^0$, i.e. the probability to miss both the decay photons of the $\pi^0 \rightarrow \gamma\gamma$ or the $e^+e^-\gamma$ system in case of π^0 Dalitz decay. The corresponding contamination of the golden sub-sample is estimated to be 13%, which can be checked by test samples extracted from the minimum bias events. The test samples consist of golden events with one (N_1) or two (N_2) converted photons pointing to the interaction vertex. Assuming the gamma identification probability to be uncorrelated for the two photons, we have $N_1 = 2N(1 - \epsilon_\gamma)\epsilon_\gamma$ and $N_2 = N\epsilon_\gamma^2$, N being the (unknown) overall rate of $p \mu^- \pi^0$ final states and ϵ_γ the photon identification efficiency; $\epsilon_\gamma = (N_1/2N_2 + 1)^{-1}$ turned out to be $(43 \pm 9)\%$. Hence, the probability of missing both gammas is $(32 \pm 10)\%$ to be compared with the MC calculation of 20.4%. Accounting for the detector livetime, trigger and selection efficiency and the sample purity, we expect 73.5 events and we observe 61.

4.2. Analysis of the kinematic distortion due to nuclear matter

In spite of the limited statistics, the golden sub-sample provides informations on the basic mechanisms that modify the kinematics of neutrino-nucleus interactions with respect to the corresponding neutrino-nucleon process. Nuclear matter perturbs the initial state of the interaction through Fermi motion; it also affects the for-

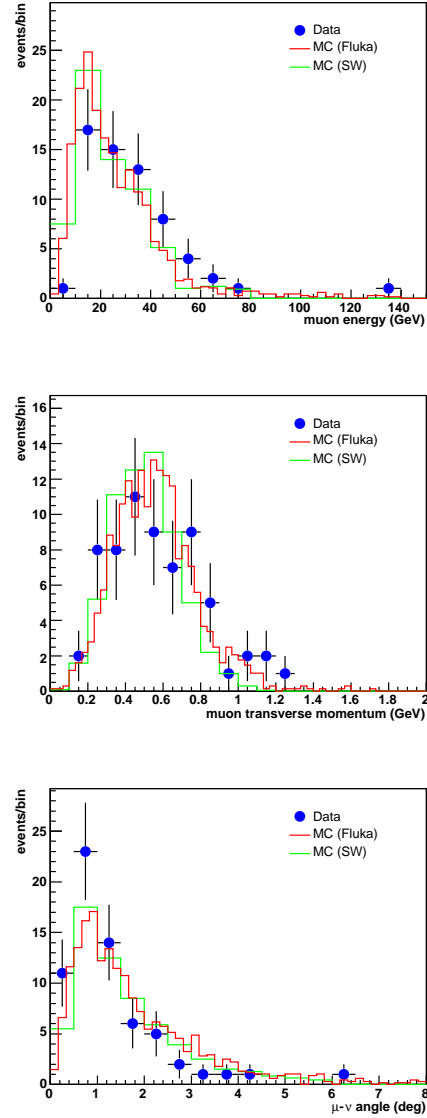


Figure 2. From top to bottom: distribution of the muon energy, muon transverse momentum and $\mu - \nu$ angle for the golden sub-sample. The continuous red (green) line is the expectation from FLUKA (Saxon-Woods) convoluted with the detector response.

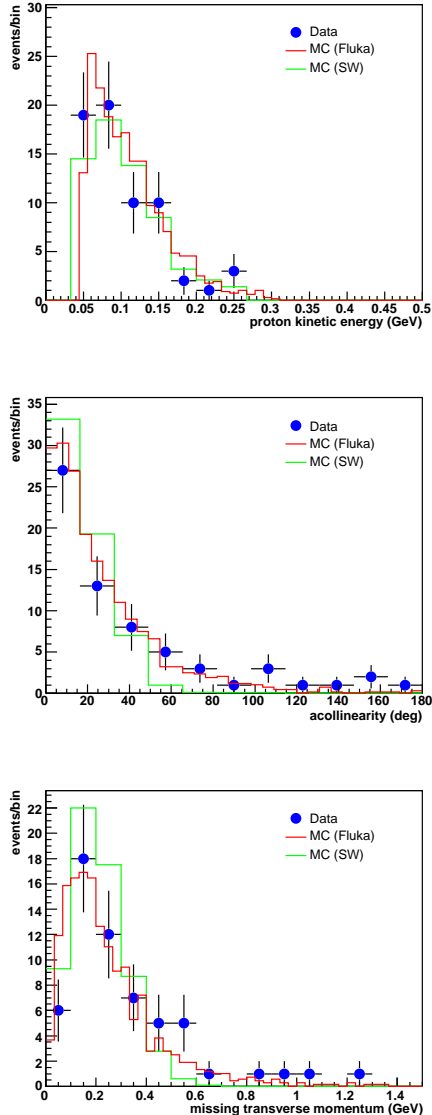


Figure 3. From top to bottom: proton kinetic energy, acollinearity and missing transverse momentum for the golden sub-sample. The continuous red (green) line is the expectation from FLUKA (Saxon-Woods) convoluted with the detector response.

mation of the asymptotic states through nuclear evaporation, hadronic re-scattering or hadronic re-absorption. Several kinematic variables are only marginally affected by nuclear matters; in this case, the corresponding distributions can be reproduced once the ν -nucleon interaction is corrected for Fermi motion and Pauli blocking using e.g. a Saxon-Woods (SW) potential for the nucleus². Clearly, purely leptonic variables belong to this category. Fig. 2 shows the distributions of muon energy, muon transverse momentum and the $\mu - \nu$ angle. Deviations from expectations are visible only for very low μ momenta and the corresponding large scattering angles. T_p (Fig. 3, top panel) is, in principle, strongly influenced by the presence of nuclear matter, but, in practice, the shape of the distribution is determined by the $T_p > 50$ MeV cut and the requirement of full containment in the fiducial volume. Figs. 2 and 3 (top panel) provide a useful consistency check, and demonstrate that MC reproduces the kinematic selection performed during the scanning and analysis of the golden sub-sample.

Other variables embedding the reconstructed kinematics of the protons are sensitive to genuine nuclear effects and should depart from the naive Saxon-Woods description. In particular, we analyzed both the acollinearity and the missing transverse momentum of the event (Fig. 3, middle and bottom panels). The former is defined as

$$A \equiv \text{acos} \left[\frac{p_{xp} p_{x\mu} + p_{yp} p_{y\mu}}{\sqrt{(p_{xp}^2 + p_{yp}^2)(p_{x\mu}^2 + p_{y\mu}^2)}} \right] \quad (1)$$

p_{xp} and p_{yp} being the transverse momentum components of the proton and $p_{x\mu}$ and $p_{y\mu}$ the corresponding quantities for the muon. For pure QE scattering on a nucleon the muon and the proton has to be back-to-back in the transverse plane so that the acollinearity is zero.

In spite of the limited statistics and the $\sim 10\%$ contamination, the imaging capability of the TPC

²In this model, nucleons are treated as a Fermi degenerate gas located in a potential well of the form $E(r) = E_0/(1 + e^{(r-R)/a})$ where a is 0.6 fm; $E_0 = 46$ MeV is the maximum well depth and R is the nuclear radius ($R = 3.6$ fm for Ar) [12].

allows to establish empirically the inadequacy of the SW description of the nucleus. An improved determination of the level of agreement between the theoretical expectations and the data can be obtained from a background subtraction procedure; this is based on the test samples mentioned in Sec.4.1. If the QE analysis is applied to the test sample where a π^0 is clearly identified, and the presence of the π^0 is then ignored, an artificial acollinearity excess is generated; in particular, 36% of the sample has $A > 60^\circ$. Similar results are obtained for p_T^{miss} where 72% of the identified resonance events shows a p_T^{miss} greater than 400 MeV. The corresponding background subtracted are shown in Fig.4. The Kolmogorov probabilities for acollinearity (transverse momentum) are 0.52 (0.30) for Fluka and 0.003 (0.027) for SW.

5. Conclusions

We discussed the first exposure of a liquid Ar TPC to a multi-GeV neutrino beam. The data provided relevant information to experimentally establish the effectiveness of the LAr technology in the reconstruction of low-multiplicity neutrino interactions. In spite of the limited size of the detector, nuclear effects beyond Fermi motion and Pauli blocking have been observed as perturbations of the quasi-elastic ν_μ CC interaction kinematics.

Acknowledgments

We thank the NOMAD and CHORUS collaborations for their support during data taking and data analysis. The presenting author (A.C.) would like to thank Bonnie T. Fleming of Yale.

REFERENCES

1. G. Acquistapace et al., CERN-ECP/95-14 (1995).
2. P. Astier et al., Nucl. Instrum. Meth. **A515** (2003) 800.
3. J. Altegoer et al., Nucl. Instr. and Meth. **A404** (1998) 96.
4. E. Eskut et al., Nucl. Instrum. and Meth. **A401** (1997) 7.

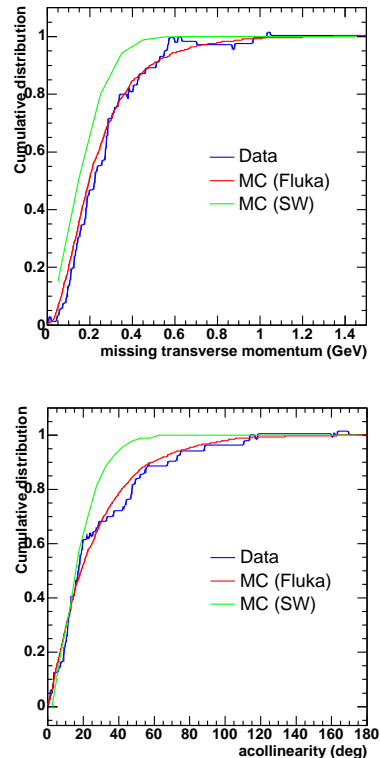


Figure 4. Background subtracted cumulative distribution of missing transverse momentum (*top*) and acollinearity (*bottom*).

5. C. Rubbia et al. [ICARUS-CERN-MI Coll.], CERN/SPSLC 96-58, SPSLC/P 304, 1996.
6. S. Ragazzi *et al.*, SPSLC/M 594, 1997
7. F. Arneodo et al., arXiv:hep-ex/9812006.
8. A. Curioni, Laurea Thesis, Milano, 1997 (in Italian); B. Boschetti, Laurea Thesis, Milano, 1997 (in Italian).
9. J. Altegoer et al., Nucl. Instrum. Meth. **A428** (1999) 299.
10. P. Cennini et al., Nucl. Instr. and Meth. **A355** (1995) 660.
11. D. Cavalli, A. Ferrari, P.R. Sala, ICARUS-TM-97/18 (1997); www.fluka.org
12. P. Balzarotti et al. ICARUS-87/27 (1987).